S1 Validation of the wet and dry sampling setups based on spike-recovery tests using red and blue polyethylene (PE) spheres

The potential for particle losses from the setups for collecting wet and dry deposition was assessed by conducting spike-recovery tests in the laboratory and in the field (at the NABEL station in Duebendorf) using red and blue spherical PE particles with nominal diameters in the range of 53-63 µm. The procedure for spiking these reference particles was as follows. Between 100 and 300 red or blue PE spheres were deposited on a glass slide using a metallic needle. An image of the glass slide was recorded with an automated optical microscope (VHX-7000, Keyence, Japan) and the number of particles were counted automatically based on a colour thresholding feature built into the microscope's software. For dry deposition samples, the glass slide was rinsed over a glass dish with ethanol using a pressurized aluminium spray to transfer the particles on the slide to the glass dish below. For wet deposition samples, first the lid of the filtration device was removed, and the outlet was connected to a vacuum pump that was switched on. Then, the glass slide was rinsed over the opening of the filtration device with ethanol using a pressurized aluminium spray bottle such that particles on the glass slide would be transferred into the filtration device and settle onto the 15 µm steel mesh fitted into it. In each case, the glass slide was inspected under the optical microscope afterwards to check if any particles remained on the glass slide. Any remaining particles were deducted from the initial particle count.

10

15

For testing the aluminium filtration device used for collecting wet deposition samples, spike-recovery experiments (n = 6) were first carried out in the laboratory to check whether particles could be lost e.g. in the gaps between individual components of the filtration device. To do so, between 100 and 300 red PE spheres were counted and added to the filtration device's 15 μ m mesh. The filtration device was disassembled, and the steel mesh was carefully removed using metal tweezers. The steel mesh was placed onto the stage of the optical microscope and an optical image of the steel mesh was recorded. The red PE spheres deposited on the steel mesh were counted. The number of red PE spheres remaining on the steel mesh was compared to the initial number of red PE spheres to compute the recovery of the red PE surrogates.

Next, similar spike-recovery experiments were performed in the field (n = 3). The filtration device was mounted onto the sampler located in the field. In the laboratory, between 100 and 300 red PE spheres were added to a glass slide and transferred to a clean 50 mL glass beaker. The beaker was covered with an aluminium foil, transported to the field, and the contents of the beaker were poured through the sampler's opening while simultaneously rinsing the inner surface of the beaker with ethanol to ensure that all particles were transferred. The on-site filtration system was switched on such that the particles would flow through the sampler and deposit onto the steel mesh fitted into the filtration device. The filtration device was then dismounted from the sampler, closed and transported back to the laboratory. There, the filtration device was disassembled, and the steel mesh was removed using metal tweezers. The number of red PE particles on the steel mesh were counted under an optical microscope. The recoveries of red PE particles were recorded.

For assessing the use of a glass dish containing glycerol for collecting dry deposition samples, three types of spike-recovery tests were carried out. These included tests with 1) glass dishes with glycerol in the field, 2) glass dishes without glycerol in the field, 3) glass dishes without glycerol and without exposure to wind in the laboratory. For the first test, between 100 and 300 red PE spheres were counted and added to a glass dish, which was then covered with a sheet of aluminium foil and transported to the field where the sampler was located. The glass dish was placed in the sampler's bucket labelled "dry", the aluminium cover was removed, and the glass dish was exposed to ambient air for two weeks. After the exposure period, the glass dish was covered with the same aluminium foil and transported back to the laboratory. There, blue PE spheres were counted and added to the dish. The contents of the dish were rinsed with ultrapure water and filtered onto a fresh stainless-steel mesh of 15 µm mesh size. An image of the steel mesh was recorded with an optical microscope and the red and blue spheres on the steel mesh were counted to assess their recoveries. The reason for adding red PE spheres before and blue PE spheres after collection was to account for possible losses of particles during sample collection and/or transport, i.e. if red PE spheres had systematically lower recoveries than those of blue PE spheres, which were of the same size range and therefore expected to behave similarly to their red-coloured counterpart, it could be attributed to losses during sample collection and/or transport. For the second test, we repeated the same procedure as above using glass dishes that did not contain glycerol.

For the third test, we repeated the same spike-recovery test with glass dishes that did not contain glycerol but were not exposed to field conditions. Instead, the glass dishes were left covered in a dark cabinet in the laboratory. This was do ne to control the influence of wind on the recoveries of the spiked particles from the glass dishes that did not contain glycerol. The effectiveness of glycerol as a particle trap was determined by comparing the recoveries of glass dishes with and without glycerol, which were exposed to similar wind speed conditions. The results from three types of tests are summarized in Table S1. The similar and high recoveries of red and blue surrogates from glass dishes containing glycerol indicate that the use of glycerol may be effective in minimizing losses of particles under windy conditions that are expected in the field.

Table S1: Recoveries of red and blue polyethylene spheres from glass dishes under different conditions, namely 1) use of glycerol as a particle trap and exposed to field conditions (e.g. wind), 2) no use of glycerol and exposed to field conditions, 3) no use of glycerol and not exposed to field conditions.

Validation experiment; dry	Average red PE	Average blue PE	Particles lost during	Maximum wind speed
deposition collection setup	recovery [%]	recovery [%]	sampling or transport?	during exposure periods
				[km/h]
Glass dish with glycerol, exposed to	87 ± 7	85 ± 6	No	22
field conditions (n = 3)				
Glass dish without glycerol, exposed	58 ± 32	74 ± 21	Yes	27
to field conditions (n = 3)				
Glass dish without glycerol, stored	83 ± 6	84 ± 7	No	Not applicable
covered in a cabinet in the lab $(n = 3)$				

S2 Thresholds applied for polymer classification in Microplastics Finder and polymer densities used in the calculation of microplastic particle mass

For the classification of polymers in Microplastics Finder based on their spectra measured via FPA-µ-FTIR, the threshold for "relevance" was set as 0.2 across all polymer types. For "similarity", polymer-specific thresholds were applied and are listed in Table S2.

Table S2: Selected threshold for similarity used in the classification of polymer using Microplastics Finder and density values used in microplastics mass calculations.

Polymer type	Threshold for "similarity"	Polymer density [g/mL]
PE	0.55	0.94
PP	0.35	0.91
PS	0.25	1.05
PET	0.35	1.39
PVC	0.55	1.4
PMMA	0.55	1.19
PU	0.65	1.21
PBT	0.75	1.32
EVAc	0.35	0.95
EVOH	0.35	1.14
ABS	0.25	1.06
PAN	0.45	1.18
PLA	0.45	1.24
POM	0.45	1.43
PC	0.45	1.21
PEEK	0.75	1.31
Silicone	0.45	1.3

S3 Features of the software platform YAMANAKA

The software platform YAMANAKA was developed to enable the routine analysis of microplastics in environmental samples based on a combination of optical microscopy and FPA-μ-FTIR. The software requires an optical image of a filter and connection to the stage of an FTIR instrument. The coordinates of the optical image are referenced with those of the stage of the FTIR instrument. The operator can then select or randomly generate areas on the optical image of the filter to analyze with the FTIR. After the analyses are finished, a matching of the optical and FTIR images is done, which enables correlative microscopy.

In addition to the matching of optical and FTIR images, the software has two optical image analysis features – the first is to count the total number of particles on the filter and the second to count the colored (red or blue) PE surrogate standards for QA/QC purposes.

To estimate the total number of particles present on an entire Anodisc filter, the optical image undergoes the following steps: smoothing and denoising of the image using a bilateral filter, conversion of the color image to grayscale, binary inversion of the image via thresholding (i.e. white particles on black background), definition of connected components (i.e. clustering of adjacent white pixels as particles) and contour detection. Each unique contour represents a unique particle. If applicable, this information is further used to determine the fraction of subsampled particles analysed with the FPA- μ -FTIR and eventually to calculate the subsampling uncertainty associated with the measurements.

For the counting of red and blue PE spherical surrogates on an Anodisc filter, we trained and implemented an object detection model based on an existing machine learning algorithm called YOLOv11 (Jocher and Qiu, 2024). Based on its performance with a validation dataset, i.e. images on which surrogates were manually annotated, the model could identify surrogate standards automatically on a whole filter in less than a minute and with an accuracy greater than 95%.

S4 Determination of level 1 uncertainties

80

Table S3: Raw data on the recoveries of red and blue PE surrogates, as well as subsampling uncertainties from the analyses of n = 59 field samples.

Sam	Red	Red PE	Red	Blue	Blue	Blue	Total no.	No.	Subsampl	No.	Ratio of	Subsam
ple	PE -	- final	PE	PE -	PE -	PE	particles	particle	ed	MPs	MPs to	pling
num	initial	count	recove	initial	final	recove	on	s in	particle	in	analyzed	uncertai
ber	count		ry [%]	count	count	ry [%]	Anodisc	subsam	fraction	subsa	particles	nty [%]
								ple	[%]	mple		
1	252	226	90	164	136	83	39616	15695	40	78	0.0050	17
2	189	128	68	146	104	71	64078	20126	31	65	0.0032	20
3	250	209	84	169	149	88	60687	19247	32	58	0.0030	21
4	264	106	40	192	85	44	52242	18654	36	46	0.0025	23
5	162	88	54	145	65	45	17748	5393	30	38	0.0070	26
6	242	207	86	161	102	63	20921	7104	34	22	0.0031	34
7	236	194	82	166	220	130	47025	15585	33	130	0.0083	14
8	201	94	47	140	88	63	55474	18119	33	24	0.0013	33
9	239	158	66	165	107	65	35259	11712	33	50	0.0043	23
10	186	158	85	146	121	83	36898	6910	19	48	0.0069	25
11	249	115	46	170	108	64	12431	3879	31	37	0.0095	27

12	174	101	58	144	79	55	27810	9463	34	51	0.0054	22
13	254	161	63	212	127	60	23797	7788	33	13	0.0017	45
14	186	73	39	142	47	33	17558	5527	31	14	0.0025	43
15	130	96	74	113	106	94	30041	9759	32	23	0.0024	34
16	257	56	22	172	47	27	36676	11785	32	11	0.0009	49
17	191	86	45	174	104	60	41023	13316	32	54	0.0041	22
18	267	102	38	228	142	62	48522	15894	33	14	0.0009	43
19	236	84	36	217	99	46	29942	9740	33	16	0.0016	40
20	144	76	53	143	92	64	51708	13475	26	17	0.0013	41
21	163	97	60	126	123	98	24624	8386	34	60	0.0072	21
22	155	80	52	156	97	62	41669	13565	33	46	0.0034	24
23	229	173	76	248	209	84	57706	18231	32	61	0.0033	21
24	197	159	81	135	121	90	32692	10601	32	35	0.0033	27
25	165	132	80	153	123	80	48546	15588	32	165	0.0106	13
26	267	160	60	228	155	68	32299	10196	32	57	0.0056	21
27	180	130	72	182	143	79	77512	24198	31	113	0.0047	15
28	189	133	70	204	175	86	51370	15831	31	48	0.0030	24
29	207	146	71	196	125	64	31682	10304	33	34	0.0033	28
30	191	154	81	200	172	86	59638	18856	32	109	0.0058	16
31	137	124	91	130	107	82	24799	7879	32	57	0.0072	21
32	192	101	53	179	99	55	33668	10569	31	32	0.0030	29
33	166	158	95	182	175	96	40072	12705	32	118	0.0093	15
34	232	149	64	196	162	83	36104	11785	33	48	0.0041	23
35	155	128	83	262	233	89	34513	11054	32	35	0.0032	27
36	162	90	56	232	143	62	36990	10984	30	25	0.0023	33
37	172	169	98	140	141	100	54160	16780	31	124	0.0074	15
38	161	106	66	188	148	79	55218	16017	29	37	0.0023	27
39	238	189	79	197	179	91	28598	9479	33	41	0.0043	25
40	130	83	64	112	66	59	33626	9929	30	47	0.0047	24
41	173	93	54	166	77	46	3941	1258	32	6	0.0048	66
42	224	168	75	222	168	76	25104	8206	33	54	0.0066	22
43	149	82	55	135	90	67	71104	22375	31	12	0.0005	47
44	218	98	45	178	74	42	11031	3504	32	27	0.0077	31

45	114	99	87	118	121	100	28064	8947	32	36	0.0040	27
46	188	73	39	170	44	26	22719	7408	33	43	0.0058	25
47	159	88	55	152	105	69	56548	18053	32	133	0.0074	14
48	234	169	72	223	182	82	31596	10059	32	26	0.0026	32
49	179	151	84	166	143	86	6466	1912	30	64	0.0335	20
50	151	111	74	171	155	91	37879	12204	32	74	0.0061	19
51	198	157	79	121	104	86	15209	5715	38	27	0.0047	30
52	197	164	83	192	146	76	12184	4051	33	88	0.0217	17
53	168	93	55	110	88	80	28615	9321	33	56	0.0060	21
54	226	179	79	205	182	89	8846	2950	33	54	0.0183	22
55	207	130	63	136	121	89	10870	3511	32	27	0.0077	31
56	205	168	82	156	144	92	15120	4999	33	94	0.0188	16
57	160	138	86	140	137	98	10212	3477	34	192	0.0552	11
58	224	46	21	117	60	51	39219	13263	34	50	0.0038	23
59	247	76	31	190	174	92	3613	1070	30	27	0.0252	31
		Mean	65		Mean	73					Mean	26
		recover			recover						subsampli	
		y of red			y of						ng	
		PE			blue PE						uncertaint	
											у	
		Standar	19		Standar	20						
		d			d							
		deviati			deviatio							
		on			n							

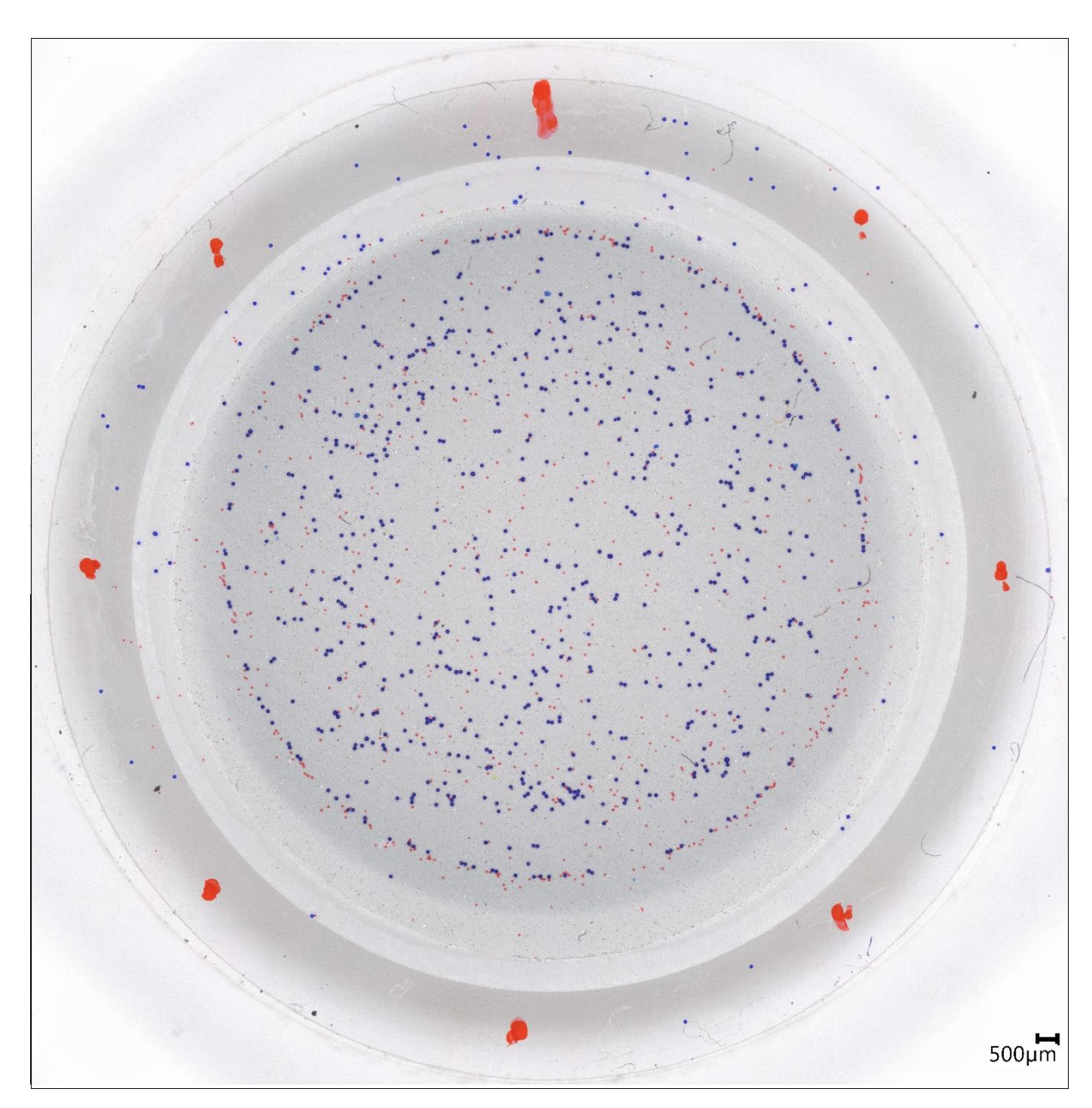


Figure S1: Anodisc filter on which red PE spheres (diameter: 53-63 μm) and blue polystyrene (PS) spheres (diameter: 104 μm) were deposited. The filter was used for the assessment of uncertainties associated with the FPA-μ-FTIR measurement device, such as repeatability or loss of optical focus due to uneven filter topography and differential particle sizes.

Table S4: Number of polymers identified by Microplastics Finder across n = 59 environmental samples at three distinct similarity thresholds. The percentage uncertainty for each polymer is calculated based on a comparison of the upper and lower number of identified polymers (based respectively on the lower and upper thresholds) with the expected value (based on the selected threshold).

Polymer	No. of MPs	No. of MPs at upper	No. of MPs at lower	Difference in no. of MPs	Relative
type	at selected	threshold (selected threshold	threshold (selected	between upper and lower	uncertainty
	threshold	+ 0.05)	threshold - 0.05)	thresholds	[%]
ABS	27	27	27	0	0
EVAc	326	312	343	31	5
EVOH	24	15	28	13	27
PAN	49	49	51	2	2
PBT	358	288	406	118	16
PC	15	15	15	0	0
PE	402	365	436	71	9
PEEK	1	1	1	0	0
PET	467	458	941	483	52
PLA	67	65	67	2	1
PMMA	128	104	157	53	21
POM	9	8	9	1	6
PP	316	308	318	10	2
PS	195	195	195	0	0
PU	106	73	154	81	38
PVC	58	44	74	30	26
silicone	73	72	76	4	3
Total MPs	2621	2399	3298	899	17

S5 Determination of level 3 uncertainties

100

To quantify the uncertainties related to the determination of the particle size (i.e., particle dimensions), which could eventually carry over into the uncertainty estimations of MP volume and mass, we determined the particles sizes (projected area equivalent circular diameters) of n = 4452 red and blue PE spheres that were added as surrogate standards to n=59 atmospheric deposition samples. The size information was extracted from optical microscopy images and FPA- μ -FTIR data using Microplastics Finder in combination with YAMANAKA.

The average diameters of 58 ± 11 µm derived from optical microscopy images and 53 ± 10 µm extracted from the FPA-µ-FTIR data generally agreed with the nominal diameter range of 53-63 µm of the red and the blue PE spheres reported

by the manufacturers of the spheres (Fig. S2). However, the sizes derived from FPA-μ-FTIR measurements were on average lower compared to those derived from optical images by 9%. A Wilcoxon signed rank test with continuity correction as well as a paired t-test on the sizes obtained from the two measurement techniques suggested that there were statistically significant differences in the sizes reported by the two techniques (p-values < 2.2e-16), we therefore consider that the length and width of the MP particles as detected by FPA-μ-FTIR are systematically too low by 9%.



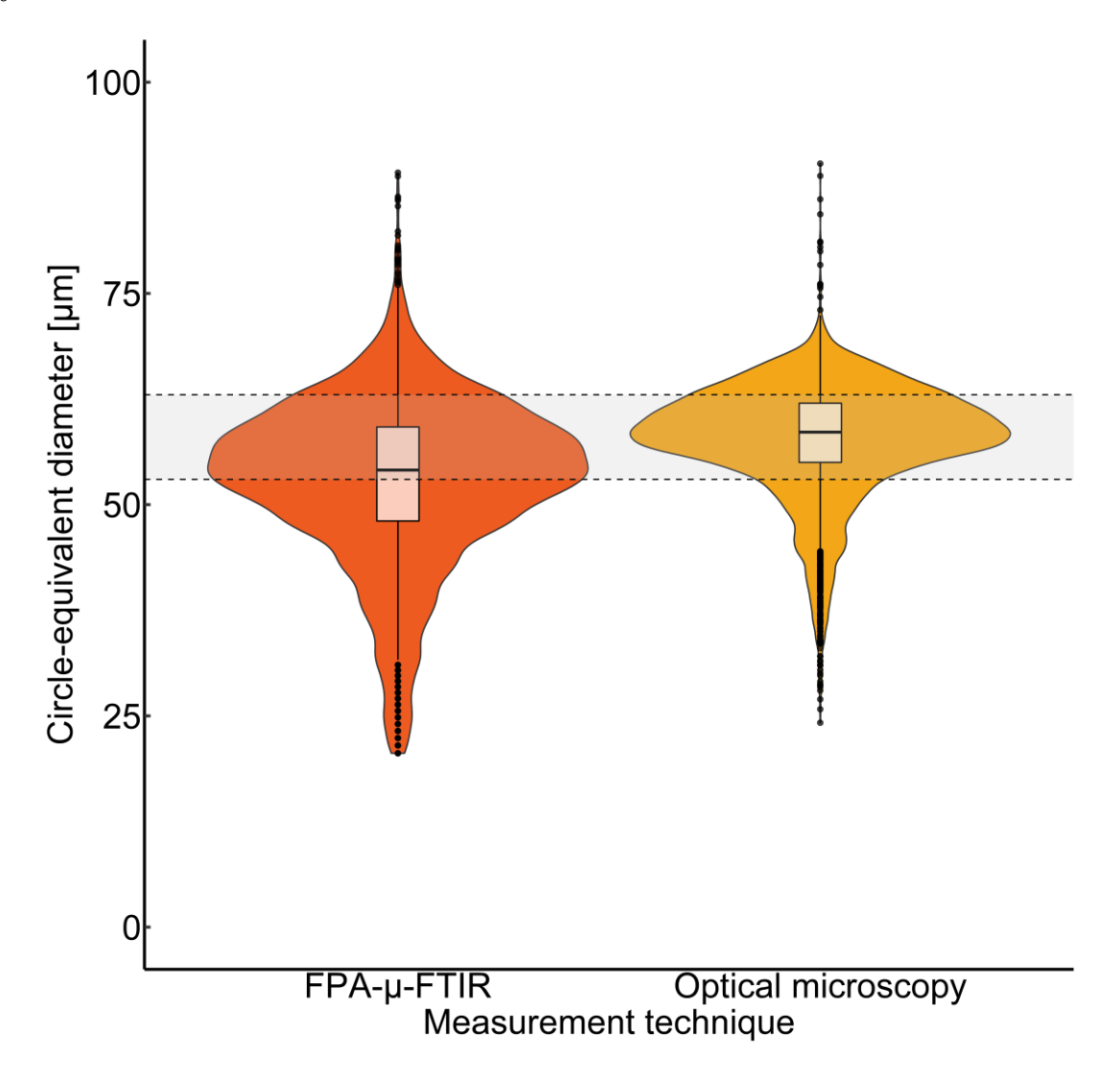


Figure S2: Comparison of circle-equivalent diameters of n = 4452 surrogate standards measured by FPA- μ -FTIR and optical microscopy. Dashed lines indicate the nominal diameter range of 53-63 μ m as declared by the supplier of the standards.

Assuming that the optical microscope provided the true size of the particles, the dimensions (length and width) of MPs identified based on FPA-μ-FTIR measurements were assumed to also be systematically underestimated by 9%. This underestimation has an impact on the volume calculation of the individual MP particles and should be considered. The ellipsoidal volumes of MP particles are smaller by a factor of (1-e_s)³ (e_s is the relative error of the size measurement, here e_s=0.09), compared to the volume of ellipsoids with the true L and W.

Applied to the test data set of Contreras et al. (2024), the erroneous measurement of L and W led to an increase of the underestimation of 1D shaped particles (from -43.7% to -53.3%), decreased the overestimation of 2D particles (from 271.0% to 142.0%) and turned the small overestimation into a small underestimation of the volume of 3D particles (from 7.7% to -7.7%). For the mixture of MP shapes in the test data set of Contreras et al. (2024), the overestimation of the total MP particle volume with erroneously measured L and W was 28.5% compared to 70.6% for the true L and W.

Table S5: Densities of polymers most frequently detected in our atmospheric deposition samples obtained from selected literature (Bellasi et al., 2021; Caldwell et al., 2022; Horton et al., 2017; Huo et al., 2022; Lusher et al., 2020).

Polymer	Minimum	Maximum	Mean density (applied in the study)	Percentage
	density	density		uncertainty
PE (incl. low- and high-density	0.89	0.98	0.94	5%
PE)				
PET	1.3	1.45	1.38	5%
PP	0.84	0.92	0.88	5%
PMMA	1.16	1.2	1.18	2%
PU	1.1	1.3	1.2	8%
PS	1.04	1.13	1.09	4%
PVC	1.16	1.58	1.37	15%

S6 Critical level and limit of detection

120

125

130

135

In analytical chemistry, the limit of detection (LOD) is considered the lowest detectable quantity or concentration of an analyte that can be differentiated from a blank measurement, i.e. a measurement of a sample where the analyte is expected to be absent. LOD is often calculated based on the mean concentration of the measured analyte in blank samples and the standard deviation of the concentrations in the measured blank samples. Often, LOD is expressed as the arithmetic mean of measured blank values plus three times the standard deviation of the blank values ($3 \cdot \sigma_B$), see e.g. Keith et al. (1983). For blank corrected measurements, the limit of detection would then simply be three times the standard deviation of the blank values. Similarly, a blank corrected limit of quantification (LOQ) is often introduced as the level above which a quantitative result can be considered as accurate, the blank corrected LOQ is then expressed as ten times the standard deviation of the blank values ($10 \cdot \sigma_B$). In this definition of LOQ, it is assumed that σ_B represents the absolute standard measurement

uncertainty also at concentrations above the LOD. The LOQ is then the concentration where the relative measurement uncertainty falls below 10%, i.e. $\sigma_B/LOQ = 0.1$.

We suggest that the above concepts for expressing LOD and LOQ should not be applied for the quantification of microplastics for the following reasons. The LOD as defined above minimizes the risk that a measured signal is interpreted as a true signal, when it is in fact not different from a blank measurement (false positive, or Type I error). It does not, however, account for false negatives (Type II error), i.e. the risk that a real signal is incorrectly interpreted as a blank measurement. In addition, the LOQ as defined above is not relevant for our study, because the measurement uncertainty of the MP analysis as proposed is largely a relative uncertainty that does not get smaller with an increasing number of detected MPs; the assumption of an absolute and constant measurement uncertainty is therefore not applicable.

140

145

150

155

160

165

170

Instead, we propose to follow the concepts of the critical level (Lc) and LOD as described by Currie (1968). According to Currie (1968), the critical level is the limit for a Type I error (false positives). The L_C is therefore conceptually identical to the LOD as defined in Keith et al. (1983). However, we propose a confidence level of 95% as an acceptable risk for a Type I error in the analysis of microplastics. The analysis of n=12 blank samples resulted in a mean number count of MPs of $m_B = 13$ with a standard deviation of $s_B = 9$ MPs. The critical level could then be calculated as 29 MPs per analysis of subsample via FPA- μ -FTIR.

The limit of detection LOD according to Currie (1968) is the threshold value above which Type I error and Type II error are minimized and can be expressed as the sum of critical level L_C and the expanded measurement uncertainty at the concentration level of the LOD, denoted as U_{LOD} . Note that U_{LOD} is expressed as absolute uncertainty and in counts of MPs per sample. For the determination of U_{LOD} , only those level 1 uncertainty components that have a direct effect on the number of MPs detected in a subsample need to be considered. In particular, the reproducibility of FTIR measurements (5%), the influence of filter topography on the FTIR measurement (24%) and the assignment or misclassification of the measured spectra (17%). Since the above components of uncertainty were determined as relative uncertainties and U_{LOD} is an absolute uncertainty, the latter must be calculated iteratively. This means that we begin with a start value for the limit of detection, calculate the corresponding U_{LOD} , update the limit of detection using Eq. (8) of the main text and continue until convergence. Finally, it is

$$U_{LOD} = q_{0.95} \cdot LOD \cdot \sqrt{0.05^2 + 0.24^2 + 0.17^2}$$

with $q_{0.95}$ the 95-quantile of the normal distribution ($q_{0.95}$ =1.645). For our analytical pipeline we find U_{LOD} to be 29 MPs and therefore a limit of detection LOD = 58 MPs.

Figure S3 shows schematically the concept of L_C and LOD as applied. Type I errors lead to an overestimation of the true MP number, whereas Type II errors lead to an underestimation of the true MP numbers. For the interpretation of the measured MPs, we consider the avoidance of a Type I error to be more important than the avoidance of a Type II error. Measurements above L_C are a reliable proof of the existence of MPs in the sample and used as the primary reporting limit. Measurements between L_C and LOD, should, however be interpreted carefully, because the increased risk for a Type II error might result in an underestimation of the true MP number in the sample.

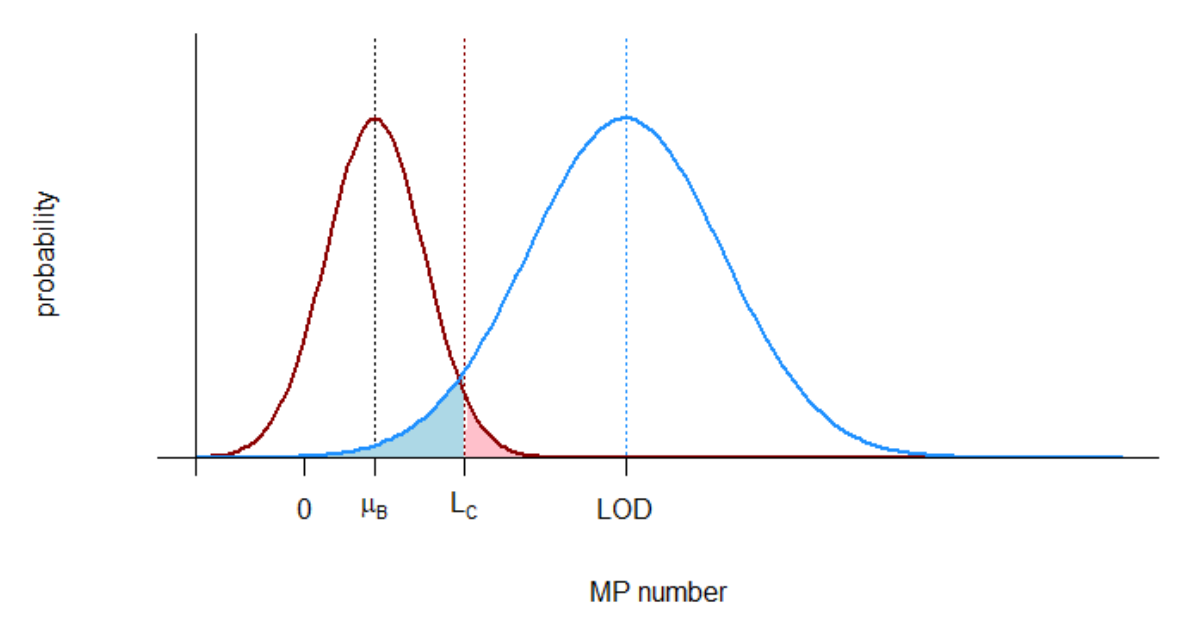


Figure S3: Schematic of the concept of L_C and LOD as applied in this study. The red area in Figure S1 indicates the probability of a Type 1 error, the blue area indicates the probability of a Type 2 error.

Figure S4 shows the mean number of different polymers found in the analysis of n = 12 blanks that were used to compute Lc and LOD.

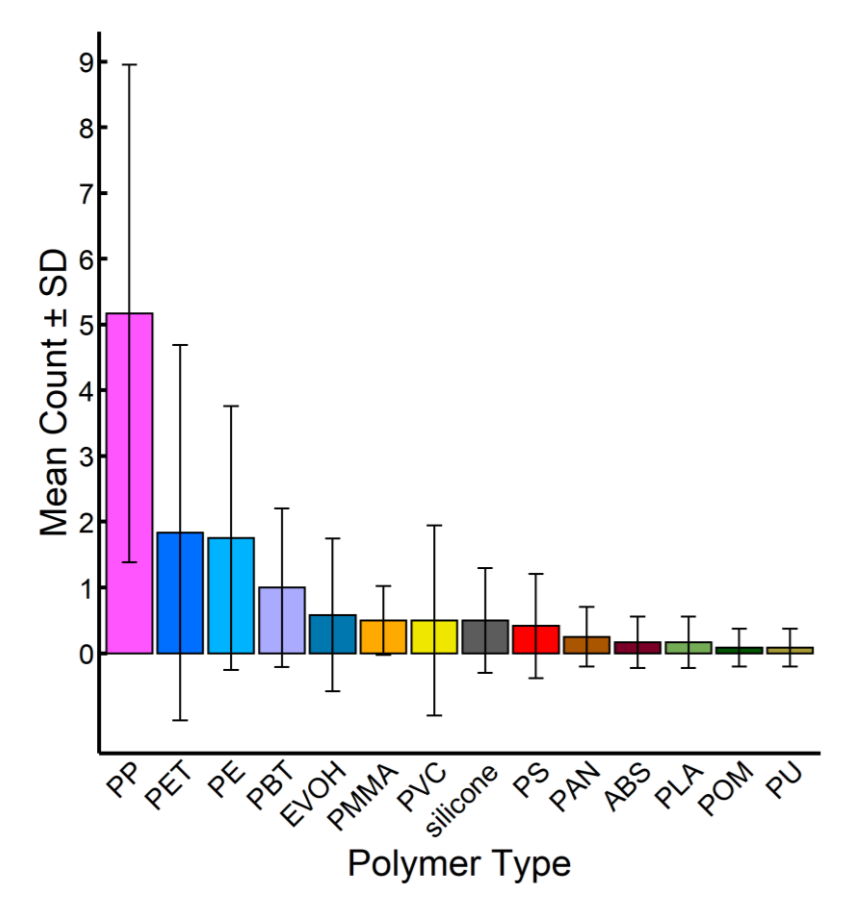


Figure S4: Average number of different polymers identified in (n = 12) blanks. PP = Polypropylene, PET = Polyethylene terephthalate, PE = Polyethylene, PBT = Polybutylene terephthalate, EVOH = Ethylene vinyl alcohol, PMMA = Polymethyl methacrylate, PVC = Polyvinyl chloride, PS = Polystyrene, PAN = Polyacrylonitrile, ABS = Acrylonitrile butadiene styrene, PLA = Polylactic acid, POM = Polyoxymethylene, PU = Polyurethane.

References

185

Bellasi, A., Binda, G., Pozzi, A., Boldrocchi, G., and Bettinetti, R.: The extraction of microplastics from sediments: An overview of existing methods and the proposal of a new and green alternative, Chemosphere, 278, 130357, https://doi.org/10.1016/j.chemosphere.2021.130357, 2021.

Caldwell, J., Taladriz-Blanco, P., Lehner, R., Lubskyy, A., Ortuso, R. D., Rothen-Rutishauser, B., and Petri-Fink, A.: The micro-, submicron-, and nanoplastic hunt: A review of detection methods for plastic particles, Chemosphere, 293, 133514, https://doi.org/10.1016/j.chemosphere.2022.133514, 2022.

Currie, L. A.: Limits for qualitative detection and quantitative determination. Application to radiochemistry, Anal. Chem., 40, 586–593, https://doi.org/10.1021/ac60259a007, 1968.

Horton, A. A., Walton, A., Spurgeon, D. J., Lahive, E., and Svendsen, C.: Microplastics in freshwater and terrestrial environments: Evaluating the current understanding to identify the knowledge gaps and future research priorities, Sci. Total Environ., 586, 127–141, https://doi.org/10.1016/j.scitotenv.2017.01.190, 2017.

- Huo, Y., Dijkstra, F. A., Possell, M., and Singh, B.: Plastics in soil environments: All things considered, in: Advances in Agronomy, Elsevier, 1–132, https://doi.org/10.1016/bs.agron.2022.05.002, 2022.
 - Jocher, G. and Qiu, J.: Ultralytics YOLO11, 2024.
 - Keith, L. H., Crummett, Warren., Deegan, John., Libby, R. A., Taylor, J. K., and Wentler, George.: Principles of environmental analysis, Anal. Chem., 55, 2210–2218, https://doi.org/10.1021/ac00264a003, 1983.
- Lusher, A. L., Munno, K., Hermabessiere, L., and Carr, S.: Isolation and Extraction of Microplastics from Environmental Samples: An Evaluation of Practical Approaches and Recommendations for Further Harmonization, Appl. Spectrosc., 74, 1049–1065, https://doi.org/10.1177/0003702820938993, 2020.